

Investigation of coherent structures in turbulent boundary layer above urban building array using proper orthogonal decomposition

Haitham Osman

Interdisciplinary Graduate School of Engineering Sciences, Kyushu University

Ikegaya, Naoki

Interdisciplinary Graduate School of Engineering Sciences, Kyushu University

<https://doi.org/10.5109/7323365>

出版情報 : Proceedings of International Exchange and Innovation Conference on Engineering & Sciences (IEICES). 10, pp.890-896, 2024-10-17. International Exchange and Innovation Conference on Engineering & Sciences

バージョン :

権利関係 : Creative Commons Attribution-NonCommercial-NoDerivatives 4.0 International

Investigation of coherent structures in turbulent boundary layer above urban building array using proper orthogonal decomposition

Haitham Osman¹, Naoki Ikegaya^{1,2}

¹ Interdisciplinary Graduate School of Engineering Sciences, Kyushu University, Japan

² Faculty of Engineering Sciences, Kyushu University, Japan

Corresponding author email: haitham.osman@kyudai.jp

Abstract: *Turbulent structures are intermittent and spatially correlated above the canopy. These structures play a crucial role in enhancing the momentum exchange inside the urban boundary layer. While various studies have explored these structures numerically and experimentally, the structures dynamics over extremely rough surfaces remain substantially less understood. Hence, this study applies Proper orthogonal decomposition (POD) to high temporal and spatial resolution data for the streamwise velocity component derived from large eddy simulation. The results reveal that the first four POD modes account for over 40% to the turbulent kinetic energy. Furthermore, the first POD pair exhibits a wider coherent structure compared to the second POD pair (mode 3 and mode 4). Interestingly, POD mode 1 and mode 2 oscillate at approximately the same frequency. This study provides deeper insights into the coherent structure's dynamics above the canopy, thereby contributing to a better understanding of the momentum exchange mechanism.*

Keywords: Large eddy simulation; Turbulent boundary layer; Coherent structure; Proper orthogonal decomposition.

1. INTRODUCTION

The characteristics of the boundary layer and the momentum or scalars exchange above the canopy are significantly influenced by the turbulent interaction between the atmosphere and the urban canopy. This flow interaction has been a central focus of numerous studies in recent years. For instance, coherent structures (i.e., organized motion) that form above the roughness garnered significant attention from researchers. These structures have been extensively studied both experimentally [1–3] and numerically [4,5]. Laboratory work has shown that these coherent structures above the canopy contribute substantially to turbulence and momentum transfer.

Wind tunnel experiments were conducted to investigate the mean flow and the turbulence structure shaped inside and above a practical shape of canopy [6]. Furthermore, Christen et al [7] performed field measurements inside and above a street canyon to specify the turbulent structure in terms of the dominant length scales. Additionally, flow over a massive urban roughness was examined to study coherent motion through comprehensive outdoor scale model experiment [8]. Moreover, Schultz and Flack studied the turbulent boundary layer, determining the structure over the rough wall from the mean flow, Reynolds stress, and high-order turbulence [9].

From a numerical simulation perspective, Watanabe [4] investigated the coherent structure of three-dimensional eddies near the top of the canopy. This study distinguished the induction of energetic perturbations in the streamwise and vertical velocities components. Additionally, direct numerical simulation were carried out to study the turbulent statistics and coherent structures by investigating the instantaneous steady flow

field and two-points correlation [10]. A large eddy simulation (LES) study was conducted for continuous and discontinuous forest canopy to inspect the turbulent structure above the canopy. The LES results showed that large-scale coherent structures were produced by the shear, and these structures are primarily seen near the canopy-free flow interface [11]. In addition, very large-scale motion was assessed in the atmospheric boundary layer using LES [12]. The power spectrum and two-point correlations depicted that the large-scale generated length in the streamwise direction is very long, about twenty times the domain height, whereas the structure length in the spanwise direction is around half the domain height. Moreover, Osman and Ikegaya investigated the effect of domain size on the turbulent structure produced above the canopy using LES [13].

The proper orthogonal decomposition (POD) method is an effective technique to extract coherent structure within turbulent flow. By linearly combining the resulting decomposed structures, termed POD modes [14], we reconstruct snapshots of the flow data. This technique has proven effective in various studies. For instance, researchers have leveraged direct numerical simulations for the velocity field to explore coherent structures in channel flow [15]. Furthermore, by utilizing POD method to vorticity fields obtained from particle image velocimetry (PIV) data, investigators have successfully examined coherent structures in water flume [16].

Recent studies have increasingly employed the POD method for investigating coherent structures over roughness surface. For example, Kellnerova et. al explored the turbulent structure within the street canyon [17]. Their analysis of PIV measurements revealed that the first POD mode, representing the vortex wake within the canyon, contained significantly higher energy

compared to subsequent modes. Moreover, researchers have utilized the POD method to examine the influence of turbulent flow mechanisms on surface drag generation over a cube array [18]. Perret and Rivet further contributed to this field by applying POD to PIV data to investigate the impact of scale on turbulent boundary layer dynamics over a cube array [19]. Demonstrating the versatility of the POD method, Liu et. al successfully extracted flow characteristics over real-urban morphology [20].

As highlighted in previous studies, examining coherent structures above canopies is crucial for understanding momentum transfer within the lower turbulent boundary layer. While experimental and numerical wind tunnel investigations have contributed to our knowledge, they have limitations in elucidating the dynamics of these turbulent structures and quantifying the contributions of different turbulent scales to their formation.

Although previous studies have examined canopy turbulence, there is a significant research gap in understanding the dominant coherent structures and their specific impacts on momentum and scalar exchange processes within the canopy environment. By leveraging the POD method, we aim to fill this gap by identifying and analyzing these coherent structures, thereby providing deeper insights into the intricate dynamics of canopy turbulence and enhancing our understanding of the exchange processes crucial for various meteorological applications.

2. METHOD

2.1 Numerical modeling

LES was conducted using an the open-source software OpenFOAM v1912 to model the turbulent flow over a staggered cubical array. Assuming incompressible flow, Navier-stokes and continuity equations were employed as shown in Table 1. The filtered continuity and momentum equations are presented in Eq. (1) and Eq. (2) respectively in Table 1. Here, u_i refers to the grid-scale (GS) streamwise, spanwise, and vertical velocity components in the i -th direction for $i = 1, 2,$ and $3,$ respectively. Here, p is the GS pressure, τ_{ij} denotes the sub-grid scale (SGS) shear stress, and ν is the kinematic viscosity.

The SGS stress was model using the standard Smagorinsky model with a constant $C_s = 0.12$, as illustrated in Eq. (3) and Eq. (4). $S_{ij} = 0.5(\partial_j u_i + \partial_i u_j)$ is the resolved strain rate tensor and ν_{SGS} is the SGS kinematic viscosity. The length scale Δ in Eq. (5) was determined based on the mesh sizes in each direction $\Delta x, \Delta y,$ and Δz . The resolved strain tensor is defined as explained in Eq. (6).

2.2 Numerical settings

The present study investigates flow over an array of cubes, each with a height of $H = 0.1m$. The

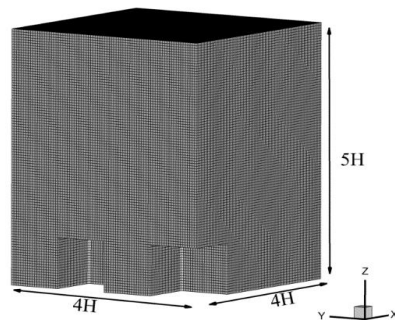


Fig. 2. Mesh resolution

cubes are arranged in a staggered pattern, as displayed in Fig. 1. The computational domain extends $4H$ in both the streamwise and spanwise directions, and its height is $5H$.

The computational domain was discretized utilizing a grid cell of $H/20$, as depicted in Fig. 2. This grid resolution, employed in previous studies [21,22], has been shown to adequately capture both the internal and external turbulent scales within and above canopy. The present study focuses on investigating the coherent structure that develops above these roughness elements.

Table 1: Fluid flow partial differential equations

Governing equation	No.
$\partial_i u_i = 0,$	(1)
$\partial_t u_i + \partial_j (u_i u_j) = -\frac{\partial_i p}{\rho} + \partial_j (\tau_{ij} + \nu \partial_j u_i).$	(2)
$\tau_{ij} - \frac{1}{3} \tau_{kk} \delta_{ij} = -2\nu_{SGS} S_{ij},$	(3)
$\nu_{SGS} = (C_s \Delta)^2 S_{ij},$	(4)
$\Delta = \sqrt[3]{\Delta x \Delta y \Delta z}$	(5)
$ S_{ij} = \sqrt{2S_{ij} S_{ij}}.$	(6)

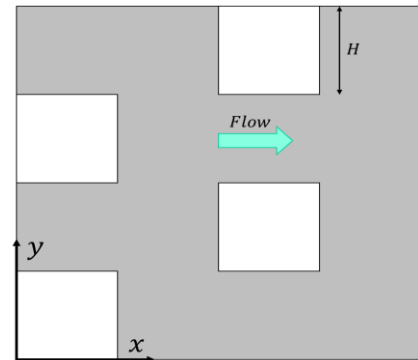


Fig. 1. the computational domain

A height variation pressure gradient, induced by the application of periodic boundary condition in streamwise and spanwise directions, drove the airflow in the domain. This pressure gradient was determined through hot-wire anemometry measurements in a wind tunnel [22,23].

The continuity and momentum equations were discretized and solved using the Pressure Implicit Method for Pressure-Linked Equations (PIMPLE) algorithm implemented in OpenFOAM. The filteredLinear2V scheme, a blend of linear and upwind interpolation methods, was employed for spatial discretization. A time step of 1×10^{-3} s, a sampling frequency 1000 kHz, and a sampling time 75s was used for the simulation. To mitigate the influence initial conditions, A pre-calculation period of 75 s was introduced before data sampling.

2.3 Proper orthogonal decomposition

POD was employed to extract coherent structures above the roughness elements. The POD method is based on decomposing the high dimensionality data, $Y(\xi, t)$, into a series of orthogonal spatial modes, $\Psi_j(\xi)$, and their temporal coefficients, $a_j(t)$, as shown in Eq. (7).

$$Y(\xi, t) = \sum_j \Psi_j(\xi) a_j(t) \quad (7)$$

Here, ξ and t denotes the spatial vector and time. Initially, a series of snapshots capturing the flow field at the designed region of interest for coherent structure analysis were extracted from the LES. In this study, the coherent structures were examined at $z = 1.2H$. These snapshots, representing the spatial and temporal variation of the flow field, are mathematically expressed as in Eq. (8)

$$Y(\xi, t) = \begin{pmatrix} u(x_1, t_1) & u(x_1, t_2) & \dots & u(x_1, t_{N_t-1}) & u(x_1, t_{N_t}) \\ u(x_2, t_1) & u(x_2, t_2) & \dots & u(x_2, t_{N_t-1}) & u(x_2, t_{N_t}) \\ \vdots & \vdots & \dots & \vdots & \vdots \\ u(x_{N_x-1}, t_1) & u(x_{N_x-1}, t_2) & \dots & u(x_{N_x-1}, t_{N_t-1}) & u(x_{N_x-1}, t_{N_t}) \\ u(x_{N_x}, t_1) & u(x_{N_x}, t_2) & \dots & u(x_{N_x}, t_{N_t-1}) & u(x_{N_x}, t_{N_t}) \end{pmatrix} \quad (8)$$

Here, $\xi = (x_1, x_2, \dots, x_{N_x})$ refers to the spatial coordinate, and $t = (t_1, t_2, \dots, t_{N_t})$ denotes the time. This study focuses on the coherent structure within the fluctuating streamwise velocity component $u'(x, y, t)$ at $z = 1.2H$. Therefore, the data matrix, Y , matrix has a

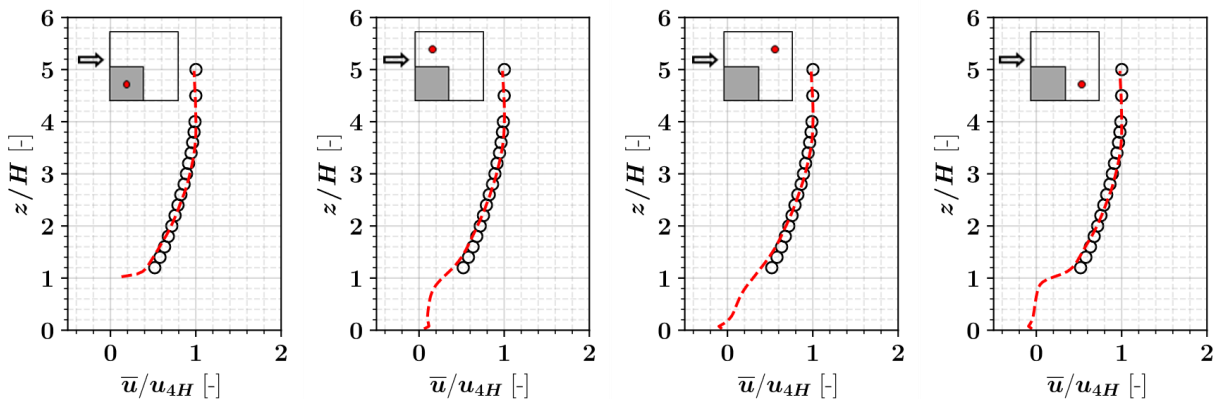


Fig. 3. Mean streamwise velocity component, \bar{u} , at four locations around the roughness element. \bar{u} is normalized by the mean streamwise velocity component at $4H$. Circles refer to the HWA results.

dimension $u'(x, y, t) \in \mathbb{R}^{N_x \times N_t}$, where N_x is the number of grid points in x and y directions, and N_t is the number of time steps. To ensure zero mean for each snapshot, a centering process for Y matrix was applied by subtracting the spatial mean vector $\bar{Y}(\xi, t)$ from all snapshots, as commonly practiced [24], the overbar denotes the spatial average. Subsequently, the POD modes were determined through an efficient singular value decomposition (SVD) as outlined in Eq. (9).

$$Y(\xi, t) - \bar{Y}(\xi, t) = USV^T, \quad (9)$$

$$U^T U = V^T V = I, \quad (10)$$

where, ϕ^T refers to the transpose of matrix ϕ . The matrices U and V are referred to the left and the right singular vectors, respectively. Here, $U \in \mathbb{C}^{N_x \times N_x}$ and $V \in \mathbb{C}^{N_t \times N_t}$ are unitary matrices with orthonormal columns. Additionally, I represents the identity matrix as defined in Eq. (10). The matrix $S \in \mathbb{R}^{N_x \times N_t}$ is a diagonal matrix with non-negative real values on the diagonal and zero elsewhere [25].

The matrix U comprises the spatial modes $\Psi_j(\xi)$, while the SV^T matrix multiplication refers the time coefficients $a_j(t)$ of POD modes. The modes are ordered sequentially, with the first mode capturing the highest energy content, followed by subsequent modes with decreasing energy contribution. The energy contribution in each mode relative to the total energy is estimated by Eq. (11). S_i indicates the diagonal i -th component of S matrix. S_i also represents the singular value of i -th POD mode. The squared values of S_i represent the kinetic energy of each mode.

$$\text{Relative contribution per mode} = \frac{S_i^2}{\sum_i S_i^2} \quad (11)$$

3. RESULTS

Mean streamwise velocity profiles at four characteristic locations relative to the roughness elements were displayed in Fig. 3. These locations encompass regions, above, between, in front of, and behind the roughness elements. To validate the LES results, the obtained velocities profiles were compared with measurements

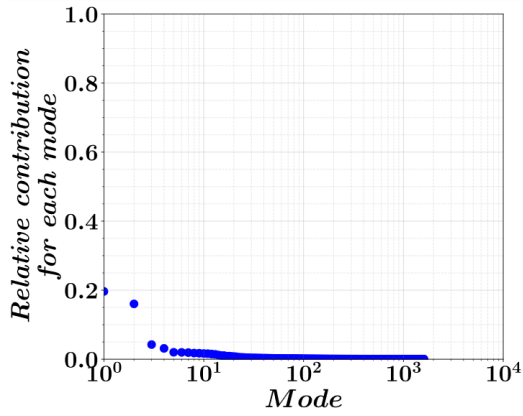


Fig. 5. Energy contained in POD modes.

from a hot-wire anemometer (HWA). For normalization purposes, the mean streamwise velocity at a height of $4H$ was used as a reference. Because of the limitations of HWA measurements within the canopy, the validation was restricted to regions above the canopy. The comparison of LES and HWA showed a high consistency.

The POD method generates an orthogonal basis for the analyzed data, referred to as modes. Fig. 4 displays the first six modes, ordered by descending energy content. The initial modes (1 and 2) exhibit large scale, broad structure. Subsequently modes (3 and 4) display progressively narrower structures while maintaining a predominantly elongated shape. This elongated structure in the first four modes is likely influenced by the limited length of the computational domain. However, a distinct

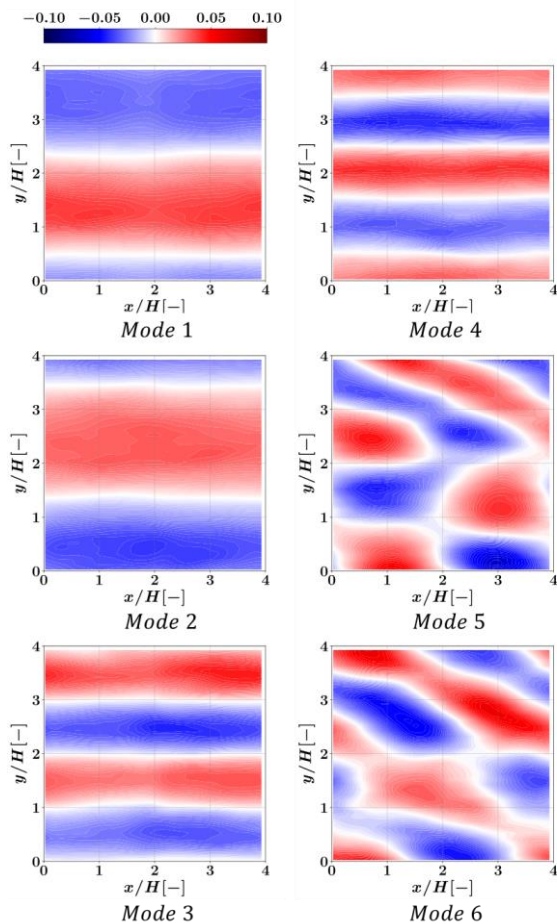


Fig. 4. The first six POD mode.

change in structure is observed in modes 5 and 6, which exhibit a tilted configuration.

The energy content per each mode is displayed in Fig. 5. The first and second modes exhibit significantly higher velocity fluctuating energy content compared to subsequent modes. Together, the first mode pair (mode 1 and 2) accounts for approximately 20% of the total energy. The energy contribution from subsequent modes decreases rapidly, with modes 3 and 4 each contributing roughly 5%. Fig. 5 indicates a lack of a dominant, singular turbulent structure within the roughness sublayer at $z = 1.2H$.

The cumulative energy associated with velocity fluctuations is presented in Fig. 6. Notably, the first three modes collectively capture 40% of the total energy. Additionally, the first ten modes account for over 50% of the total energy, and this proportion exceeds 80% when considering the first 100 modes

The cumulative energy distribution in Fig. 6 illustrates the presence of multiple scales within the flow above the roughness elements. While the initial large-scale modes (1, 2, and 3) exert significant influence, the smaller-scale modes also contribute substantially to the overall turbulent energy within the roughness sublayer at $z = 1.2H$.

The temporal coefficients $a_j(t)$ associated with each POD mode are depicted in Fig. 7. The time axis is normalized by the total sampling time of 75s. Notably, the first mode pair (mode 1 and 2) exhibited similar temporal fluctuation coefficients patterns, as shown in Fig. 7. Moreover, a comparable trend is observed for the second (modes 3 and 4) and third (modes 5 and 6) mode pairs.

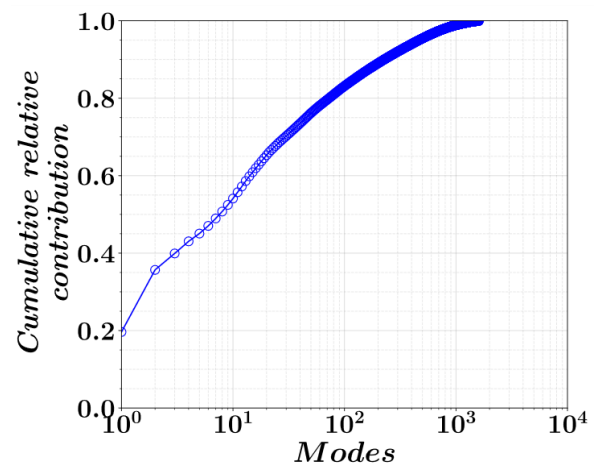
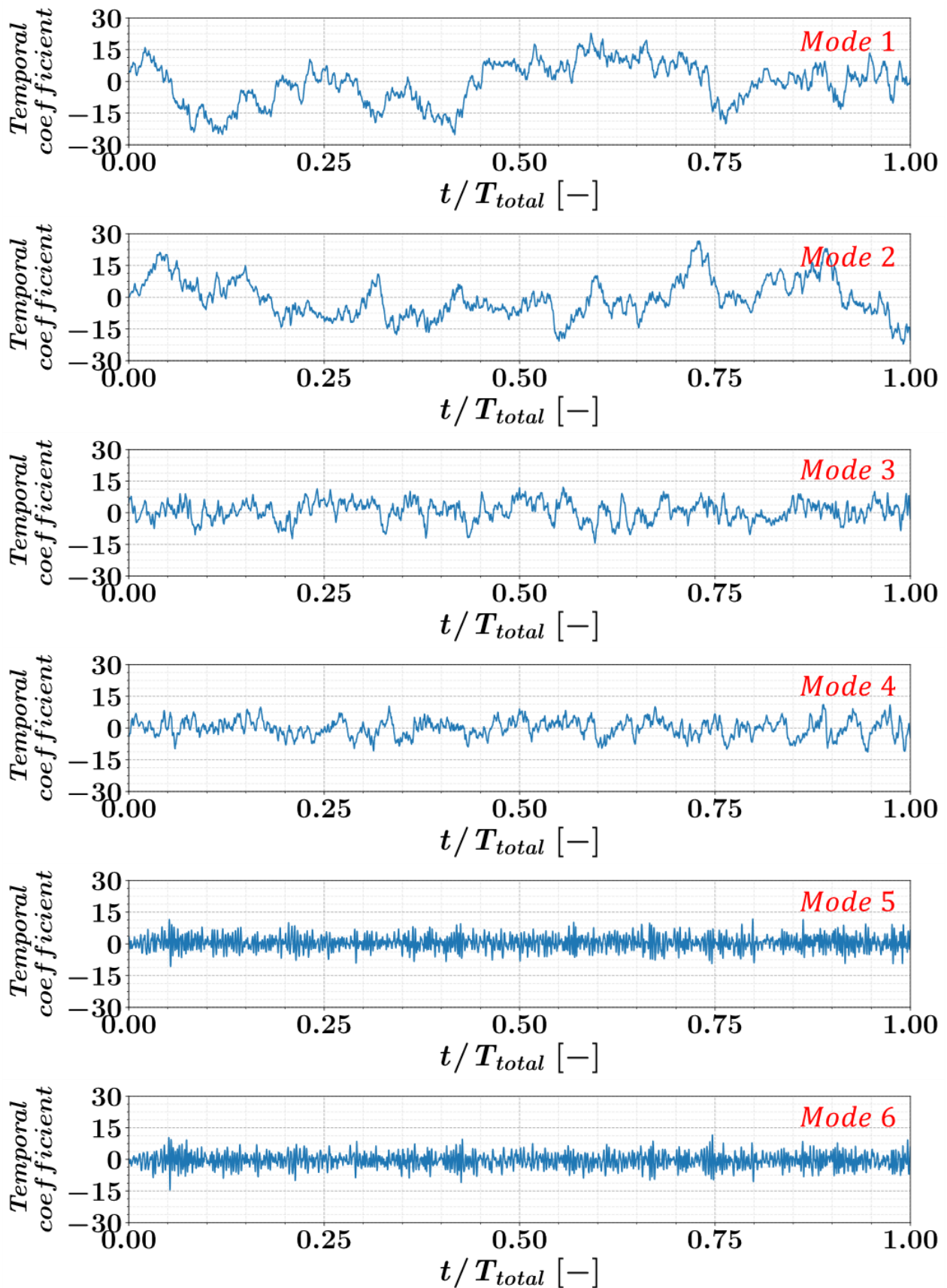


Fig. 6. Cumulative energy contained in POD modes.



s

The Welch periodogram method was utilized to estimate the energy spectrum. This involves splitting the temporal coefficient into overlapping multiple segments, applying a window function to each segment, and subsequently averaging the resulting spectra [26]. In this study, the number of segments is 20% the total length of the temporal coefficient, while there is an

overlap between the segments by 10% of the temporal coefficient length.

Fig. 8 illustrates the energy spectra of the temporal coefficient for the POD modes. The first mode pair (mode 1 and 2) indicated the lowest frequency while encompassing the highest energy content. The

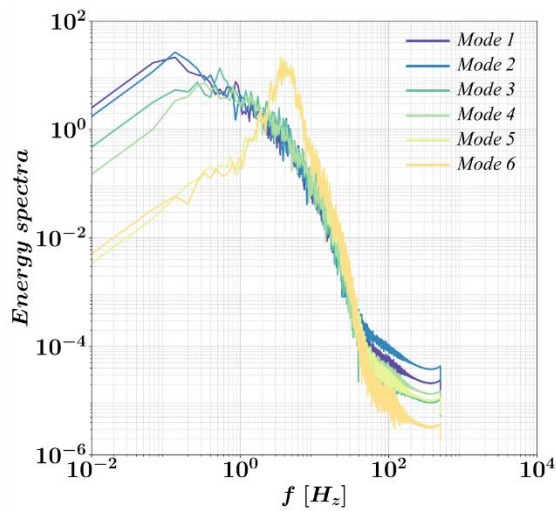


Fig. 8. Energy spectra of temporal coefficient for the first tenth POD modes.

subsequent mode pairs (modes 3 and 4, and modes 5 and 6) display progressively higher dominant frequencies.

4. CONCLUSION

This study investigated the characteristics of turbulent flow dynamics over a canopy through the application of POD. By decomposing the flow field into orthogonal modes (i.e., basis), we successfully identified the dominant coherent structures and quantified their contributions to the turbulence dynamics at a height of $z = 1.2H$ above the canopy. Our findings reveal that the first ten POD modes collectively capture over 60% of the total turbulent kinetic energy. Notably, the initial four modes exhibit elongated, large-scale coherent structures above the canopy. However, the first pair modes (mode 1 and mode 2) showed the widest turbulent structure compared with the subsequent modes. Furthermore, the analysis of temporal coefficients associated with the first six POD modes indicated distinct frequency bands. The first and second mode pairs share similar temporal fluctuations, while the third mode pair displays higher frequencies. These results underscore the multi-scale nature of turbulence in this environment, with both large-scale coherent structures and smaller-scale fluctuations playing significant roles in momentum and energy transfer processes within the canopy boundary layer.

5. REFERENCES

[1] M. Horiguchi, T. Hayashi, A. Adachi, S. Onogi, Large-Scale Turbulence Structures and Their Contributions to the Momentum Flux and Turbulence in the Near-Neutral Atmospheric Boundary Layer Observed from a 213-m Tall Meteorological Tower, *Boundary-Layer Meteorol.* 144 (2012) 179–198.

[2] A. Christen, E. van Gorsel, R. Vogt, Coherent structures in urban roughness sublayer turbulence, *Int. J. Climatol.* 27 (2007) 1955–1968.

[3] M.R. Raupach, J.J. Finnigan, Y. Brunei, Coherent eddies and turbulence in vegetation canopies: The mixing-layer analogy, *Boundary-Layer Meteorol.* 78 (1996) 351–382.

[4] T. Watanabe, Large-Eddy Simulation of

Coherent Turbulence Structures Associated with Scalar Ramps Over Plant Canopies, *Boundary-Layer Meteorol.* 112 (2004) 307–341.

[5] K. Gavrilov, G. Accary, D. Morvan, D. Lyubimov, S. Méradji, O. Bessonov, Numerical Simulation of Coherent Structures over Plant Canopy, *Flow, Turbul. Combust.* 86 (2011) 89–111. z.

[6] P. Kastner-Klein, M.W. Rotach, Mean Flow and Turbulence Characteristics in an Urban Roughness Sublayer, *Boundary-Layer Meteorol.* 111 (2004) 55–84.

[7] A. Christen, E. van Gorsel, R. Vogt, Coherent structures in urban roughness sublayer turbulence, *Int. J. Climatol.* 27 (2007) 1955–1968.

[8] A. Inagaki, M. Kanda, Organized Structure of Active Turbulence Over an Array of Cubes within the Logarithmic Layer of Atmospheric Flow, *Boundary-Layer Meteorol.* 135 (2010) 209–228.

[9] M.P. Schultz, K.A. Flack, The rough-wall turbulent boundary layer from the hydraulically smooth to the fully rough regime, *J. Fluid Mech.* 580 (2007) 381–405.

[10] J.H. Lee, H.J. Sung, P.-A. Krogstad, Direct numerical simulation of the turbulent boundary layer over a cube-roughened wall, *J. Fluid Mech.* 669 (2011) 397–431.

[11] K. Gavrilov, G. Accary, D. Morvan, D. Lyubimov, S. Méradji, O. Bessonov, Numerical Simulation of Coherent Structures over Plant Canopy, *Flow, Turbul. Combust.* 86 (2011) 89–111.

[12] J. Fang, F. Porté-Agel, Large-Eddy Simulation of Very-Large-Scale Motions in the Neutrally Stratified Atmospheric Boundary Layer, *Boundary-Layer Meteorol.* 155 (2015) 397–416.

[13] H. Osman, N. Ikegaya, Minimum Requirements for Reproducing Urban Turbulent Boundary Layer Over a Cube Array Using Les for Pedestrian-Level Wind Prediction, Available SSRN <https://ssrn.com/abstract=4886551> (2024).

[14] Z. Liu, R.J. Adrian, T.J. Hanratty, Large-scale modes of turbulent channel flow: transport and structure, *J. Fluid Mech.* 448 (2001) 53–80.

[15] P. Moin, R.D. Moser, Characteristic-eddy decomposition of turbulence in a channel, *J. Fluid Mech.* 200 (1989) 471–509.

[16] R. Gurka, A. Liberzon, G. Hetsroni, POD of vorticity fields: A method for spatial characterization of coherent structures, *Int. J. Heat Fluid Flow* 27 (2006) 416–423.

[17] R. Kellnerova, L. Kukacka, V. Uruba, K. Jurcakova, Z. Janour, Detailed analysis of POD method applied on turbulent flow, *EPJ Web Conf.* 25 (2012) 01038.

[18] M.A. Ferreira, B. Ganapathisubramani, Scale interactions in velocity and pressure within a turbulent boundary layer developing over a staggered-cube array, *J. Fluid Mech.* 910 (2021) A48.

[19] L. Perret, C. Rivet, Dynamics Of A Turbulent Boundary Layer Over Cubical Roughness

Elements: Insight From PIV Measurements And Pod Analysis, in: Proceeding Eighth Int. Symp. Turbul. Shear Flow Phenom., Begellhouse, Connecticut, 2013: pp. 1–6.

- [20] Y. Liu, C.-H. Liu, G.P. Brasseur, C.Y.H. Chao, Proper orthogonal decomposition of large-eddy simulation data over real urban morphology, *Sustain. Cities Soc.* 89 (2023) 104324.
- [21] T. Sanemitsu, N. Ikegaya, T. Okaze, J.J. Finnigan, Appropriate Momentum Provision for Numerical Simulations of Horizontally Homogeneous Urban Canopies Using Periodic Boundary Conditions, *Boundary-Layer Meteorol.* 188 (2023) 485–522.
- [22] H. Osman, Muhd Azhar Zainol, N. Ikegaya, Statistical analysis of turbulent flow over a building array using LES, *Proc. Int. Exch. Innov. Conf. Eng. Sci.* 9 (2023) 429–434.
- [23] A.B.Z. Muhd, W. Wang, N. Ikegaya, Similarity of the Extreme Wind Profiles within Urban Turbulent Boundary Layers of Uniform and Non-Uniform Height Block Arrays, (2024).
- [24] M.A. Mendez, A. Ianiro, B.R. Noack, S.L. Brunton, eds., *Data-Driven Fluid Mechanics*, Cambridge University Press, 2023.
- [25] S. L. Brunton, K. J. Nathan, eds., *Data-Driven & Engineering Machine Learning, Dynamical Systems, and control*, First edit, 2017.
- [26] Z. Jin, Q. Han, K. Zhang, Y. Zhang, An intelligent fault diagnosis method of rolling bearings based on Welch power spectrum transformation with radial basis function neural network, *J. Vib. Control* 26 (2020) 629–642.